SOLID-STATE SYNTHESIS OF POWDERS OF Ni–Cr AND Ni–Mo ALLOYS

Iryna KUD[*], Roman MEDIUKH[*], Oleksandr MYSLYVCHENKO[*], Roman LYTVYN[*], Larysa KRUSHYNSKA[*], Vira MEDIUKH[*], Oleksandr BASHTA[**], Pavlo NOSKO[**], Ostap ZGALAT-LOZYNSKYY[*]

[*]Frantsevich Institute for Problems in Materials Science, National Academy of Sciences of Ukraine, Omeljan Pritsak Str., 3, 03142 Kyiv, Ukraine
[**]Aerospace Faculty, Department of Applied Mechanics and Materials Engineering, State University "Kyiv Aviation Institute", 1, Lubomyr Huzar Ave., 03058 Kyiv, Ukraine

vallllly9996@gmail.com, roman.mediukh@gmail.com, zvyagina47@gmail.com, rovalit@ukr.net, krush.ipms@gmail.com, vira.mediukh@gmail.com, nosko_p@ukr.net, oleksandr.bashta@npp.kai.edu.ua, o.zgalatlozynskyi@ipms.kyiv.ua

received 21 January 2026, revised 29 May 2026, accepted 31 May 2026

Abstract: The features of phase formation in Ni–Cr and Ni–Mo solid solutions during interaction of the components of Ni–20 wt% Cr and Ni–20 wt% Mo powder mixtures by high-temperature vacuum treatment and mechanical alloying were investigated. During high-temperature treatment, FCC nickel-based solid solutions formed due to diffusion of chromium or molybdenum into the nickel lattice. Diffusion interaction started at 1000°C and completed at 1200°C with formation of homogeneous Ni–Cr or Ni–Mo solid solutions. Mechanical alloying behavior strongly depended on the alloying element. Homogeneous FCC Ni–20 wt% Cr solid solution powder with a particle size of 50–100 μm was obtained after 15 h of low-energy milling in a Pulverisette 6 planetary mill. In contrast, complete homogenization of the Ni–20 wt% Mo system was not achieved even after 60 h of milling. The obtained results demonstrate that mechanical alloying is more efficient for Ni–Cr powders, whereas high-temperature vacuum synthesis is more suitable for obtaining homogeneous Ni–Mo solid solutions.

Key words: refractory alloys, nickel, chromium, molybdenum, high temperature synthesis, mechanical alloying

1. INTRODUCTION

To Superalloys are traditionally classified according to the main matrix-forming element into nickel-, iron–nickel-, and cobalt-based systems [1–3]. Among them, nickel-based superalloys are widely used as structural materials for aerospace applications [4] and as protective coatings operating under severe conditions [5–9]. Due to their excellent high-temperature strength, fatigue resistance, creep resistance, fracture toughness, corrosion and oxidation resistance, nickel-based superalloys can operate for long periods at temperatures approaching 1400°C without significant softening or degradation. Therefore, such materials are extensively used in the hottest sections of jet and rocket engines, including turbine blades, discs, combustion chambers, and afterburners [4].

Nickel-based superalloys are generally divided into solid-solution-strengthened and precipitation-hardened alloys according to their strengthening mechanism [10]. Solid-solution-strengthened alloys are characterized by high-temperature corrosion resistance and good weldability, whereas precipitation-hardened alloys exhibit superior high-temperature strength and creep resistance [10].

Nickel-based superalloys commonly contain substantial amounts of alloying elements, including Cr, Al, Ti, Co, Mo, W, Ta, Hf, and Nb, which provide solid-solution and precipitation strengthening as well as improved oxidation and corrosion resistance [10].

Conventional production routes for nickel superalloys involve vacuum induction melting (VIM) followed by vacuum arc remelting (VAR) or electroslag remelting (ESR). In some cases, triple melting routes combining VIM, ESR, and VAR are applied to improve chemical homogeneity and structural quality [11]. In integrated vacuum induction melting and inert gas atomization (VIM–IGA) processes, the molten alloy is atomized using high-pressure inert gas to produce spherical powder particles with improved chemical homogeneity.

The superalloys produced by casting are often characterized by chemical segregation and non-uniform grain structures. The grain size can be optimized and controlled by thermomechanical processing, in which deformation is carried out at temperatures sufficiently high to promote recovery and recrystallization, leading to grain refinement and homogenization of the microstructure. Hot working followed by cold deformation and annealing enables formation of a uniform recrystallized structure with improved mechanical properties. Appropriate control of thermomechanical processing parameters, such as temperature, strain, and strain rate, is essential to avoid excessively fine grains that reduce creep resistance and excessively coarse grains that deteriorate tensile strength, fatigue resistance, and ductility [12–14].

Powder metallurgy methods make it possible to overcome many limitations of ingot metallurgy, particularly segregation and thermal cracking during hot working, and enable the production of highly homogeneous powders [15]. One of the most effective powder metallurgy techniques is mechanical alloying (MA) [16]. During MA, severe plastic deformation and defect accumulation promote solid-state diffusion and phase transformations, resulting in the formation of solid solutions, intermetallic compounds, or amorphous phases.Nickel-based superalloy powders are commonly

 DOI: 10.65731/ama/2026-0043

consolidated by hot isostatic pressing, hot extrusion, and isothermal forging processes [17].

Mechanical alloying is a solid-state powder processing technique in which powder particles undergo repeated welding, fracture, and rewelding in a high-energy ball mill. During mechanical alloying, metallic powders, typically in elemental form, are mixed and subjected to severe plastic deformation. Under high-energy milling conditions, initially crystalline metal powders experience intensive collisions with milling balls, leading to particle agglomeration and formation of fine lamellar structures [16].

During mechanical alloying of metallic systems, continuous formation of fresh surfaces creates favorable conditions for solid-state interaction between the components. Simultaneously, deformation-induced diffusion processes promote alloying at the atomic level, resulting in the formation of solid solutions, intermetallic compounds, or even amorphous phases [16]. Optimization of mechanical alloying parameters should ensure a dynamic balance between particle fracture and cold welding processes [16].

Previous studies demonstrated the possibility of obtaining Ni–Cr and Ni–Mo solid solutions by mechanical alloying. López-Báez et al. [18] synthesized nanostructured Ni–20Cr alloy powders after 30 h of high-energy milling in Simoloyer CM01 horizontal attritor with a duty cycle consisting of 3 minutes of operation at a rotational speed of 1800 rpm and 1 minute of operation at 1000 rpm. It was shown that interfacial diffusion and diffusion along dislocations and subgrain boundaries controlled the alloying process. Dekhil et al. [19] reported of formation nanocrystalline Cr50Ni50 material during high-energy milling of Cr–Ni mixtures in Fritsch Pulverisette 7 planetary mill at room temperature under argon atmosphere at a ball-to-powder weight ratio of 35:3 and speed of 400 rpm. After 25 h of milling, the interdiffusion between Cr and Ni atoms led to the formation of a mixture of disordered FCC Ni–Cr and BCC Cr–Ni solid solutions.

Oleszak et al. [20,21] investigated mechanical alloying of Ni–Mo powder mixtures containing 20 and 43 at% Mo using both high-energy Fritsch P5 planetary ball mill at a rotation speed of 240 rpm in argon and low-energy mill at a rotational speed of 90 rpm in air at a ball-to-powder weight ratio of 10:1 and 40:1, respectively. In the case of the Ni–20 at% Mo composition processed in a high-energy Fritsch P5 mill, formation of an FCC Ni–Mo solid solution with a lattice parameter of 0.3612 nm and a minimum crystallite size of approximately 30 nm was reported. In contrast, low-energy milling in air resulted in slower alloying kinetics due to oxygen contamination during treatment. For the Ni–43 at% Mo mixtures, both high- and low-energy mechanical alloying led to formation of bimodal structures consisting of amorphous and nanocrystalline molybdenum phases with crystallite sizes of about 20 nm.

Previous investigations also showed that preliminary mechanical activation of powder mixtures can substantially reduce synthesis temperature by 300–400°C and improve powder dispersion [22,23]. In particular, mechanical activation enabled solid-state synthesis of Ni–Cr–Al–Y alloys at temperatures as low as 1000°C [24].

The Ni–Cr [25] and Ni–Mo [26] systems are characterized by wide concentration ranges of substitutional solid solutions. Since Ni, Cr, and Mo remain in the solid state up to 1200°C, formation of Ni–Cr and Ni–Mo substitutional solid solutions may proceed through solid-state diffusion mechanisms. During MA, severe plastic deformation and defect accumulation promote solid-state diffusion and phase transformations, resulting in the formation of solid solutions, intermetallic compounds, or amorphous phases.

However, comparative studies of phase formation kinetics in Ni–Cr and Ni–Mo systems under identical conditions of vacuum synthesis and mechanical alloying remain limited. In particular, the influence of alloying element nature on solid-state interaction mechanisms and homogenization efficiency requires further clarification.

The aim of the present work was to establish the features of phase formation and alloying kinetics in Ni–20 wt% Cr and Ni–20 wt% Mo systems under identical conditions of high-temperature vacuum synthesis and mechanical alloying and to determine the influence of alloying element nature on the efficiency of solid-state homogenization.

2. MATERIALS AND METHODS

The main structural characteristics and physical properties of the components used for solid-state synthesis of Ni–Cr and Ni–Mo solid solutions are summarized in Table 1.

Tab. 1. Structural characteristics and physical properties of the investigated systems [27]

System	Lattice and atomic radius, R (nm)		ΔR/R, (%)	Diffusion parameters		Melting point (°C)
	Matrix element	Alloying element		Dself-diff. ($cm^2 \cdot s^{-1}$)	Dself-diff. ($cm^2 \cdot s^{-1}$)	
Ni–Cr	α-Ni FCC, 0.124	Cr BCC, 0.128	4.0	Ni 1.0 (900–1250°C) Cr $6.47 \cdot 10^{-2}$ (1050–1350°C)	Ni→Cr $3.5 \cdot 10^{-4}$ (870–1150°C) Cr–Ni 5.45 (350–600°C) Cr–Ni 0.3 (600–900°C)	1455 for Ni 1903 for Cr
Ni–Mo	α-Ni FCC, 0.124	Mo BCC, 0.139	12.1	Ni 1.0 (900–1250°C) Mo 1.1 (1850–2350°C)	Ni–Mo $1.6 \cdot 10^{-3}$ (900–1200°C) Mo–Ni 3.1 (1000–1500°C)	1455 for Ni 2617 for Mo

The data presented in Table 1 indicate that at temperatures up to 1200°C the diffusion rates of nickel in chromium and molybdenum are approximately three orders of magnitude lower than the diffusion rates of chromium and molybdenum in nickel. Therefore, during solid-state interaction, chromium and molybdenum are expected to diffuse predominantly into the nickel matrix. According to the Hume–Rothery rules, the smaller atomic radius mismatch in the Ni–Cr system and the negative enthalpy of mixing favor formation of substitutional solid solutions and may provide more favorable alloying kinetics compared with the Ni–Mo system.

The starting materials used in the present study were electrolytic chromium powder EPKh (99.99% purity), molybdenum powder PM99.95 (99.95% purity) with a maximum particle size of 10 μm, and electrolytic nickel powder PNE (99.8% purity) with an average particle size of approximately 40 μm (Fig. 1).

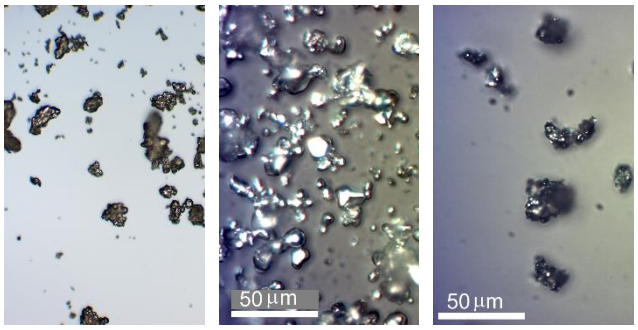

a) b) c)

Fig. 1. Morphology of the initial powders: a) Ni; b) Cr; c) Mo

The commercial Kh20N80 powder was produced by conventional melting and atomization process.

The reaction mixtures were prepared to obtain Ni–20 wt% Cr (mixture 1) and Ni–20 wt% Mo (mixture 2) solid solutions. The powder mixtures were homogenized and mechanically treated in a Pulverisette 6 planetary mill using a stainless-steel vial and steel balls (diameter 8 mm) in ethanol at a ball-to-powder weight ratio of 5:1.

Phase formation behavior in the Ni–Cr and Ni–Mo systems was investigated during high-temperature vacuum synthesis from micron-sized metal powder mixtures. Prior to thermal treatment, mixtures 1 and 2 were briquetted at a pressure of 150 MPa. High-temperature solid-state synthesis was carried out in an SNV–1.3,1/20–I1 electric vacuum furnace under a residual pressure of approximately 1×10^{-3} Pa in the temperature range of 900–1200°C with an isothermal holding time of 2 h.

The formation of solid solutions in the Ni–Cr and Ni–Mo systems was also investigated during mechanical alloying of the powder mixtures.

The characteristic features of solid-state interaction during mechanical alloying were studied as functions of milling vial rotational speed, treatment time, and ball-to-powder weight ratio. Mechanical alloying was carried out in a Pulverisette 6 low-energy planetary mill under argon atmosphere at a rotational speed of 400 rpm using 4 mm diameter steel balls and a ball-to-powder weight ratio of 10:1. The treatment duration was 5, 10, and 15 h for the Ni–Cr system and 20, 40, and 60 h for the Ni–Mo system.

To improve homogenization efficiency and reduce powder sticking to the milling balls and vial walls, mechanical alloying in the Pulverisette 6 mill was additionally performed in reverse mode with alternating rotation direction every 5 min.

High-energy mechanical alloying was also carried out in an AIR high-energy mill under argon atmosphere at a rotational speed of 1370 rpm for both systems for 0.5 h using 15 mm diameter steel balls.

X-ray diffraction (XRD) analysis was performed in reflection mode using a Proto AXRD stage diffractometer equipped with a Cu-Kα radiation source, a rotatable sample stage, and a DECTRIS hybrid pixel detector. The obtained diffraction patterns were processed using the PowderCell software package.

The microstructure and morphology of the synthesized powders were examined using a Tescan MIRA3 LMU scanning electron microscope (Tescan, Czech Republic) equipped with an X-Max 80 EDXS system and INCA software (Oxford Instruments, UK). Additional microstructural observations were carried out using an LMM–3000 vertical metallographic microscope. The EDXS results were normalized to 100%.

3. RESULTS AND DISCUSSION

3.1. High-temperature solid-state synthesis in vacuum

The XRD analysis data for the products obtained during solid-state interaction of the initial components are presented in Table 2.

Tab. 2. XRD analysis data for the products of solid-state interaction in the Ni–Cr and Ni–Mo systems

Regime of interaction		XRD analysis data			
Temperature (°C)	Holding time (h)	Phase composition	Cubic lattice constant, *a** (nm)	Phase composition	Cubic lattice constant, *a** (nm)
		Ni–Cr system		Ni–Mo system	
900	2	Ni	0.351	Ni	0.350
		Cr	0.288	Mo	0.314
1000	2	Ni	0.356	Ni	0.355
		Cr	0.288	Mo	0.314
1100	2	Ni–Cr	0.360	Ni–Mo	0.358
1200	2	Ni–Cr	0.361	Ni–Mo	0.360

*Reference lattice constants: a = 0.352 nm for Ni, a = 0.288 nm for Cr, and a = 0.315 nm for Mo [27]

 DOI: 10.65731/ama/2026-0043

The XRD results presented in Table 2 show that after heat treatment at 900°C the products contain only the initial metallic components with lattice constants corresponding to the reference data, indicating the absence of noticeable solid-state interaction. Increasing the synthesis temperature to 1000°C initiates diffusion processes, as evidenced by an increase in the lattice parameter of nickel, whereas the lattice constants of chromium and molybdenum remain unchanged.

The observed distortion of the nickel crystal lattice is associated with diffusion of chromium and molybdenum atoms into the nickel matrix due to differences in atomic radii between Ni, Cr, and Mo [27]. Further increasing in temperature intensifies the solid-state interaction process. After heat treatment at 1100°C, the diffraction patterns contain only one FCC phase corresponding to Ni–Cr or Ni–Mo solid solutions. The lattice parameter of the nickel-based phase continues to increase and reaches its maximum value after synthesis at 1200°C.

The SEM observations of the samples obtained during high-temperature vacuum synthesis (Figs. 2 and 3) are consistent with the XRD results.

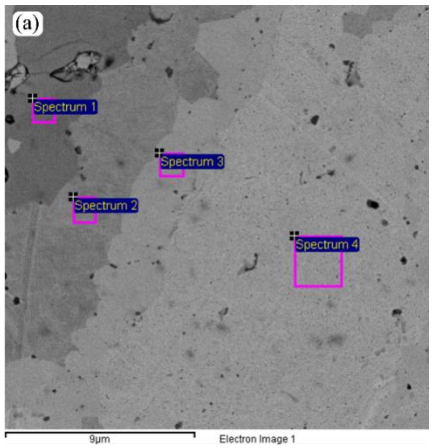

Spectr.	Element (wt%)	
	Cr	Ni
1	100	–
2	94.5	5.5
3	57.6	42.4
4	38.8	61.2

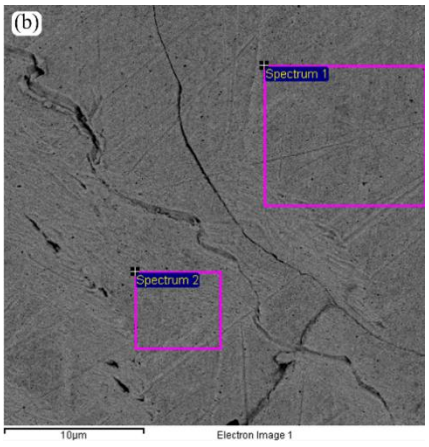

Spectr.	Element (wt%)	
	Cr	Ni
1	14.7	85.3
2	14.4	85.6

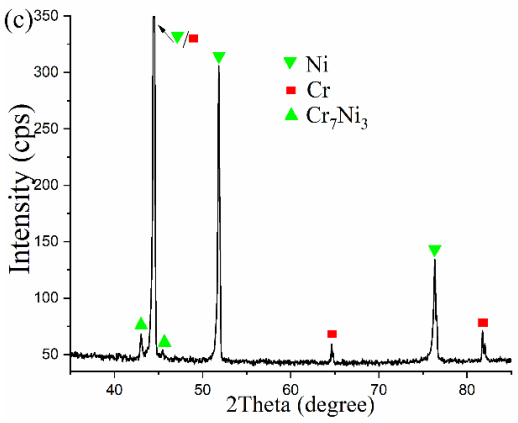

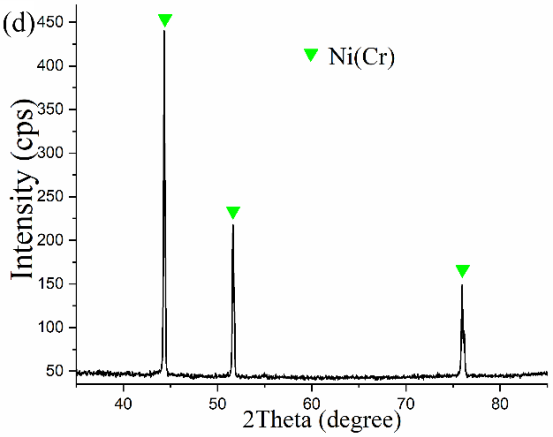

Fig. 2. SEM micrographs and XRD patterns of Ni–20 wt% Cr samples after 2 h heat treatment in vacuum at (a, c) 1000°C and (b, d) 1200°C

The SEM and EDXS analyses of the Ni–20 wt% Cr sample synthesized at 1000°C (Fig. 2a, b) demonstrate the onset of solid-state interaction in the system, which is confirmed by the presence of regions with different chemical compositions. The dark-grey areas correspond to chromium-rich regions containing nearly 100 wt% Cr, whereas the light-grey regions correspond to Ni-based solid solutions with different chromium contents formed due to diffusion of chromium into nickel.

EDXS analysis of local regions in the sample synthesized at 1200°C revealed chromium contents in the range of 14–15 wt%. This discrepancy relative to the nominal composition may be associated with local compositional heterogeneity and limitations of local microanalysis. At the same time, XRD analysis (Fig. 2c, d) confirmed formation of a single FCC solid solution phase.

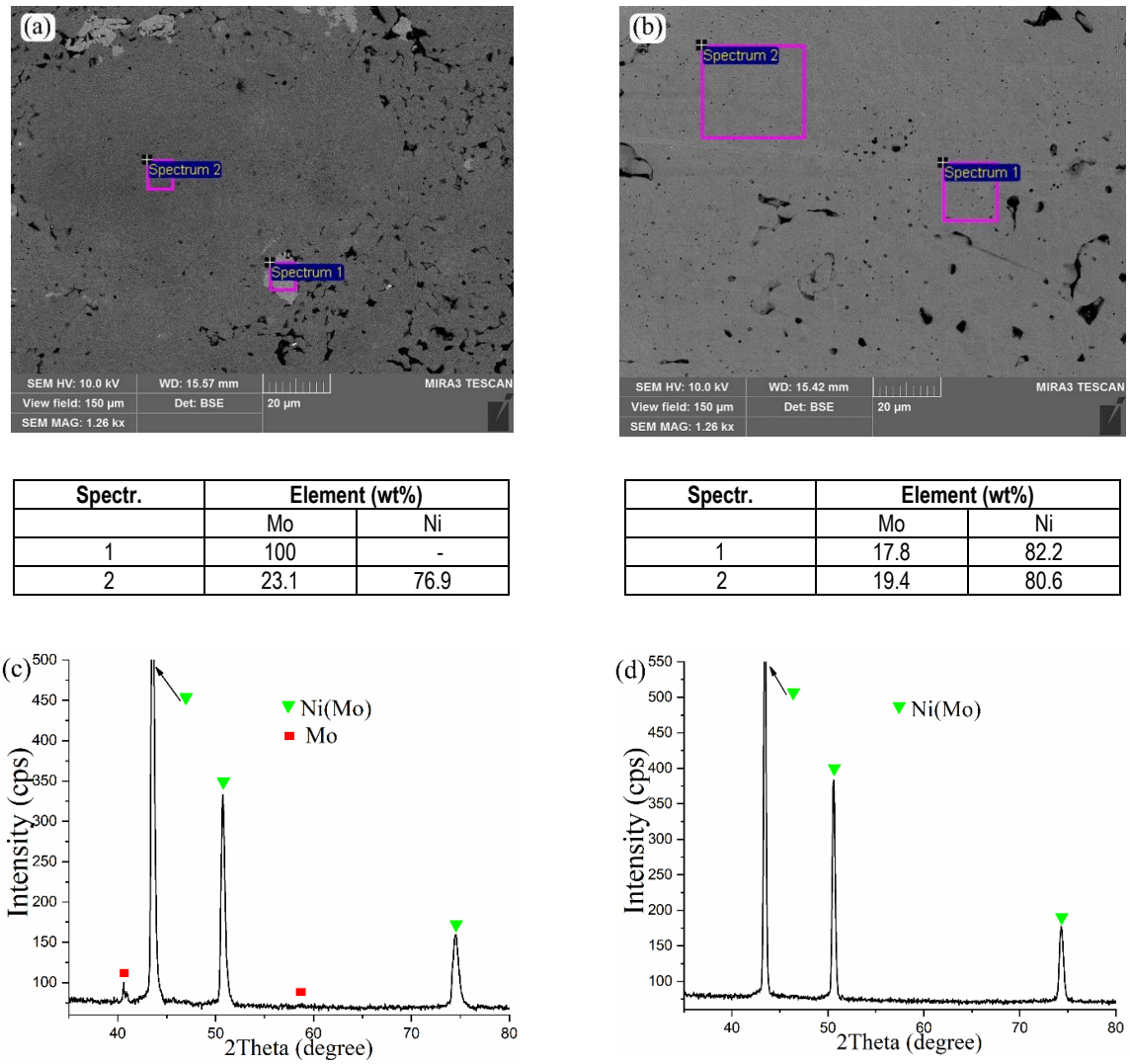

Spectr.	Element (wt%)	
	Mo	Ni
1	100	-
2	23.1	76.9

Spectr.	Element (wt%)	
	Mo	Ni
1	17.8	82.2
2	19.4	80.6

Fig. 3. SEM micrographs and XRD patterns of Ni–20 wt% Mo samples after 2 h heat treatment in vacuum at (a, c) 1000°C and (b, d) 1200°C

The SEM micrographs of the Ni–20 wt% Mo sample heat-treated at 1000°C (Fig. 3a, b) show the presence of both dark and light regions. According to the EDXS results, the dark regions correspond to a Ni–23.1 wt% Mo solid solution formed by diffusion of molybdenum into nickel, whereas the light regions correspond to residual molybdenum particles. These observations indicate that solid-state interaction in the Ni–Mo system starts at 1000°C.

Increasing the synthesis temperature to 1200°C resulted in formation of a homogeneous Ni–Mo solid solution with a molybdenum content close to the nominal composition. The SEM observations are consistent with the XRD results shown in Fig. 3c, and 3d.

The obtained results indicate that heat treatment at 1200°C for 2 h ensures formation of homogeneous nickel-based solid solutions in both investigated systems.

3.2. Mechanical alloying

Table 3 summarizes the XRD and EDXS results obtained for the products of mechanical alloying in the Ni–20 wt% Cr and Ni–20 wt% Mo systems.

The iron contamination observed in the mechanically alloyed powders is associated with abrasive wear and friction between the powder particles, stainless-steel milling balls, and milling vessel walls during treatment. Increasing the milling time to 60 h resulted in an approximately threefold increase in Fe content (Table 3).

According to the XRD results, mechanical alloying of the Ni–20 wt% Cr mixture in the AIR high-energy mill at a rotational speed of 1370 rpm for 0.5 h in pulse charge mode led to formation of an Ni–Cr solid solution, which is confirmed by the increase in the lattice parameter of the nickel-based phase.

SEM analysis showed that the mechanically alloyed Ni–Cr powder consisted of large flake-like agglomerates with sizes ranging from 100 to 1000 µm (Fig. 4a). Figure 4b presents a fragment of an agglomerate formed by particles of Ni–Cr solid solution with different chromium contents. According to the EDXS data, the agglomerates are compositionally heterogeneous. Small amounts of Cr-rich regions are also observed on the surface of the agglomerates, indicating incomplete homogenization during short-term high-energy treatment.

 DOI: 10.65731/ama/2026-0043

Tab. 3. XRD and EDXS data for the products obtained by mechanical alloying of Ni–20 wt% Cr and Ni–20 wt% Mo mixtures

Mechanical synthesis mode			Phase composition and lattice constants (nm)	Elemental composition (wt%)					Particle size (μm)
n (rpm)	$\tau_{treat.}$ (h)	d_{ball} (mm)		Ni	Cr	Mo	Fe	O	
Ni–Cr mixture									
1370	0.5	15	Ni–Cr (0.357)	–	–	–	–	–	100–1000
400	5	4	Ni (0.350) Cr (0.288) Ni–Cr (0.354)	72.8	25.1	–	0.9	1.2	150–250
	10	4	Ni–Cr (0.359)	75.1	21.8	–	1.7	1.4	50–100
	15	4	Ni–Cr (0.361)	75.5	20.8	–	1.8	1.9	50–100
Ni–Mo mixture									
1370	0.5	15	Ni (0.351) Mo (0.314)	–	–	–	–	–	100–1000
400	20	4	Ni–Mo (0.355) Mo (0.314)	85.0	–	10.9	2.2	1.9	–
	40	4	Ni–Mo (0.358) Mo (0.314)	83.9	–	10.2	3.8	2.1	–
	60	4	Ni–Mo (0.359) Mo (0.314)	83.5	–	8.7	6.3	2.5	50–100

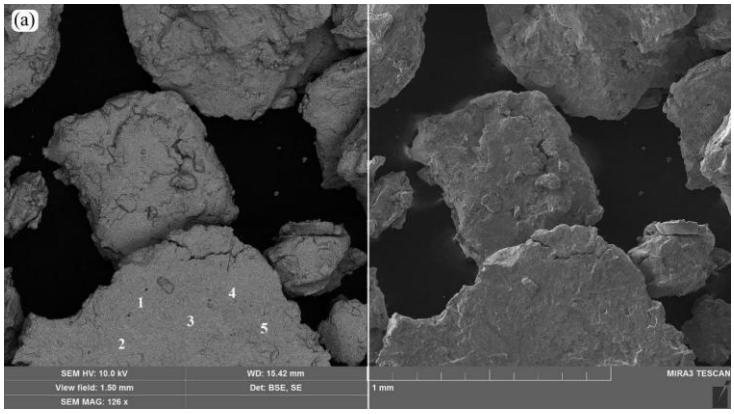

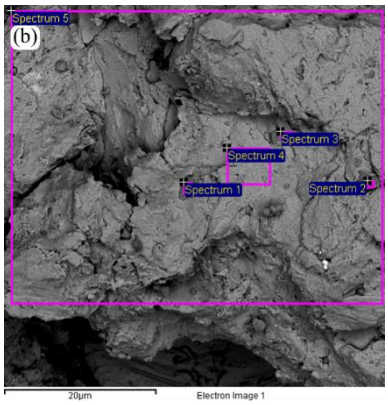

Spectr.	Element (wt%)		
	Cr	Fe	Ni
1	93.5	-	6.5
2	93.8	-	6.2
3	18.3	0.8	80.9
4	16.5	-	83.5
5	24.0	-	76.0

Fig. 4. (a) SEM image and (b) EDXS elemental analysis of Ni–Cr powder obtained by mechanical alloying in the AIR high-energy mill at a rotational speed of 1370 rpm

The XRD results for the Ni–20 wt% Mo mixture mechanically alloyed in the AIR mill indicate the presence of only the initial metallic components with lattice parameters corresponding to the reference values [25]. These results demonstrate the absence of noticeable solid-state interaction and indicate that short-term high-energy treatment is insufficient for formation of a homogeneous Ni–Mo solid solution. This behavior is associated with the larger atomic radius mismatch between Ni and Mo compared with the Ni–Cr system (Table 1).

Fig. 5 shows the milling balls with a diameter of 15 mm after mechanical alloying in the AIR high-energy mill. In the Ni–Mo system (Fig. 5b), layered agglomerates formed during the initial stage of mechanical alloying as a result of severe plastic deformation and cold welding processes. Intensive adhesion promoted both

agglomeration of the powder mixture and sticking of flake-like particles to the milling balls, resulting in formation of spherical surface crusts.

In the Ni–Cr system, the powder particles adhered to the vessel walls in the form of continuous layers and formed nearly continuous crusts on the milling balls. In contrast, the Ni–Mo system exhibited formation of discontinuous island-like surface crusts. Mechanical alloying in the AIR mill was accompanied by significant powder losses reaching up to 20 wt% even after 0.5 h of treatment.

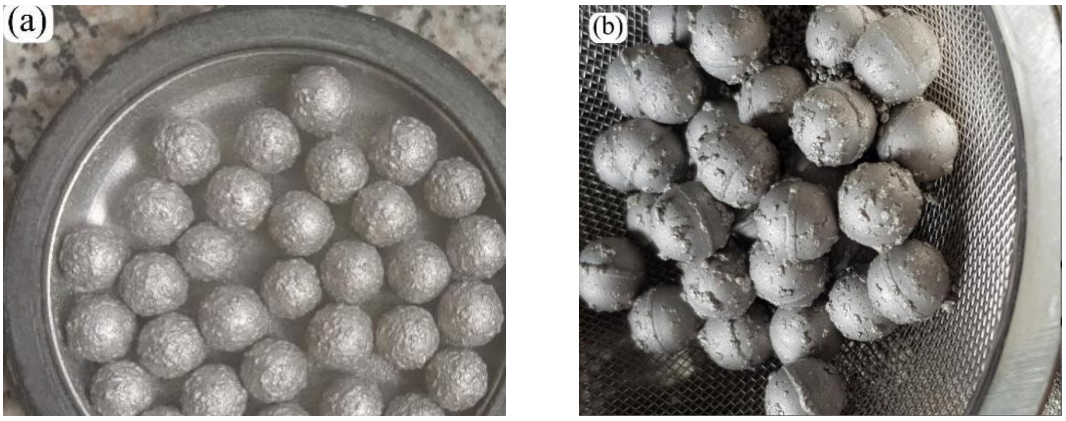

Fig. 5. Milling balls after mechanical alloying of (a) Ni–20 wt% Cr and (b) Ni–20 wt% Mo mixtures in the AIR planetary mill

The differences in solid-solution formation behavior between the Ni–Cr and Ni–Mo systems are associated with the different physicochemical properties of chromium and molybdenum, including their electronic structure, atomic size mismatch, solubility range in nickel, and melting temperatures.

According to the XRD results, mechanical alloying of the Ni–20 wt% Cr mixture in the Pulverisette 6 mill for 5 h resulted in formation of an Ni–Cr solid solution together with residual initial components (Table 3). This is confirmed by the increase in the lattice parameter of the nickel-based phase relative to pure nickel (Fig. 6).

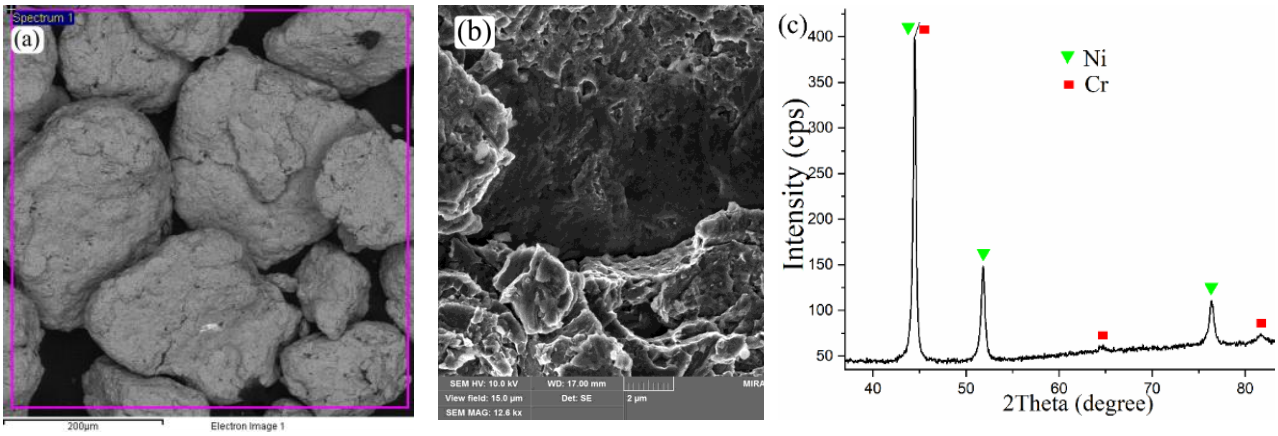

Element (wt%)					
N	O	Si	Cr	Fe	Ni
0.8	1.1	0.3	27.7	0.8	69.3

Fig. 6. SEM image of the Ni–20 wt% Cr powders obtained by mechanical alloying for 5 h at a rotational speed of 400 rpm in the Pulverisette 6 planetary mill (a, b) and corresponding XRD pattern (c).

According to the SEM analysis, the mechanically alloyed product consists of heterogeneous agglomerates with a relatively smooth morphology and sizes ranging from 50 to 200 µm (Fig. 6a).

The SEM image of a representative agglomerate (Fig. 6b) shows that it is composed of particles with sizes from 1 to 6 µm, including both residual initial components and Ni-based solid-solution particles with different chromium contents. The morphology of several fragments indicates formation of a layered structure during mechanical alloying.

According to the XRD results, formation of the Ni–Cr solid solution occurred after 10 h of treatment. Increasing the mechanical alloying time to 15 h resulted in formation of a homogeneous Ni–Cr solid solution (Table 3). The SEM observations shown in Fig. 7 confirm the improved homogeneity of the mechanically alloyed powder.

The morphology evolution of the powders mechanically alloyed for 5, 10, and 15 h is presented in Fig. 7. After 10 h of treatment, a noticeable decrease in particle size is observed, whereas the agglomerate size remains nearly unchanged with further increase in milling time up to 15 h. The Ni–Cr powder obtained after 15 h of mechanical alloying consists of rounded agglomerates with sizes of 50–100 µm formed by particles with sizes ranging from 0.2 to 5 µm (Fig. 7c)

The commercial Kh20N80 powder consists of agglomerates formed by tightly bonded fine rounded particles with sizes ranging from 10 to 50 µm (Fig. 7d).

 DOI: 10.65731/ama/2026-0043

The XRD pattern of the Ni–20 wt% Cr mixture mechanically alloyed in the Pulverisette 6 mill for 15 h (Fig. 8a) confirms formation of a single-phase Ni–Cr solid solution. EDXS analysis performed on local regions as well as over larger areas (50 × 50 μm) demonstrated a homogeneous distribution of alloying elements throughout the powder particles (Fig. 8b). In addition to the nickel matrix, chromium (20.6–21.1 wt%), iron (0.7–1.8 wt%), and oxygen (1.8–1.9 wt%) were detected in the mechanically alloyed powder (Fig. 8b).

EDXS analysis of the commercial Ni–Cr powder revealed the presence of fine oxide inclusions at grain boundaries depleted in chromium and containing approximately 11 wt% oxygen (31 at%) (Fig. 8c). The elevated oxygen content in the Kh20N80 commercial powder is associated with surface oxidation during manufacture by the atomization method.

The EDXS results indicate that the Ni–Cr powder obtained by mechanical alloying exhibits higher compositional homogeneity compared with the commercial Kh20N80 powder.

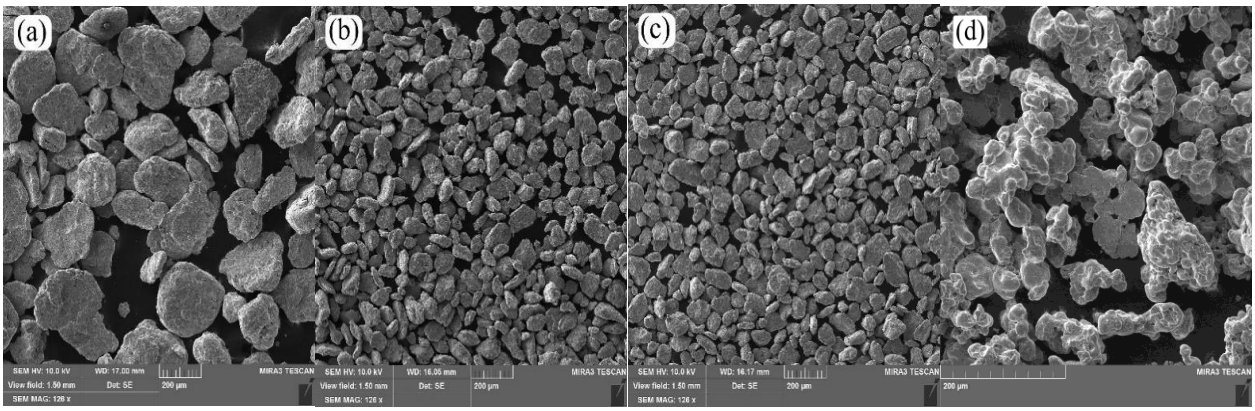

Fig. 7. SEM images of Ni–20 wt% Cr powders obtained by mechanical alloying for (a) 5 h, (b) 10 h and (c) 15 h in the Pulverisette 6 planetary mill at a rotational speed of 400 rpm and of (d) Kh20N80 commercial powder

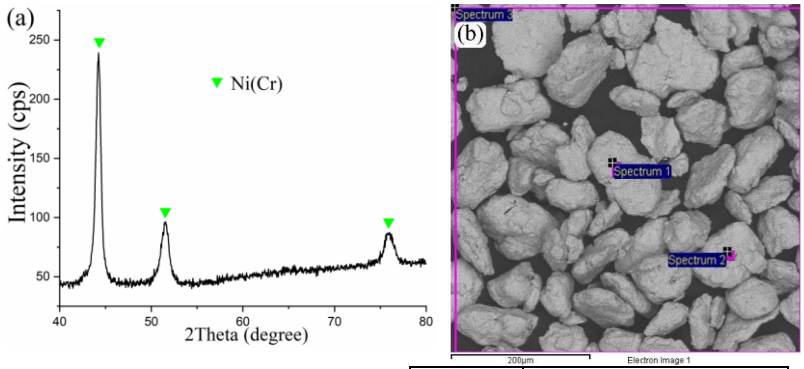

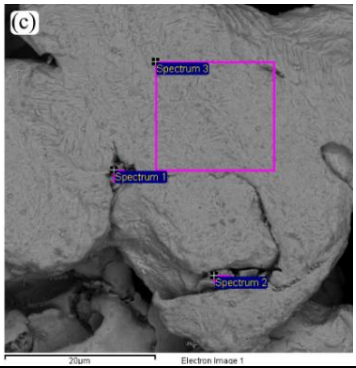

Spectr.	Element (wt%)			
	O	Cr	Fe	Ni
1	1.8	20.6	1.3	76.3
2	1.8	21.1	0.7	76.4
3	1.9	20.8	1.8	75.5

Spectr.	Element (wt%)				
	O	S	Ca	Cr	Ni
1	11.1	0.3	-	5.8	82.7
2	11.2	0.4	0.5	3.7	84.2
3	2.0	-	-	14.5	83.5

Fig. 8. (a) XRD pattern, (b) SEM image and EDXS analysis of the Ni–Cr solid solution powder obtained by mechanical alloying in the Pulverisette 6 planetary mill for 15 h, and (c) commercial Kh20N80 powder

The obtained results demonstrate the effectiveness of using the Pulverisette 6 mill in reverse mode for mechanical alloying of the Ni–Cr mixture. Alternating the rotation direction influenced the motion trajectories of the milling balls and reduced the time required for formation of a homogeneous Ni–Cr solid solution to 15 h, which is approximately two times shorter than the treatment duration reported in [18].

Under the selected processing conditions, a dynamic balance between particle fracture, cold welding, and solid-solution formation was achieved through diffusion of chromium into the nickel matrix. In addition, powder adhesion to the milling balls and vessel walls was significantly reduced during treatment (Fig. 9).

Investigation of mechanical alloying in the Ni–Mo system was performed considering both the present results obtained in the AIR high-energy mill and previously reported data [20,21] describing long-term low-energy milling exceeding 100 h. Therefore, mechanical alloying of the Ni–Mo mixtures in the present work was carried out for relatively long treatment times of 20, 40, and 60 h.

The XRD results for the Ni–Mo system (Table 3) show that formation of an Ni–Mo solid solution with a lattice parameter of 0.355 nm occurred after 20 h of treatment at a rotational speed of 400 rpm. Increasing the mechanical alloying time to 60 h resulted in a gradual increase in the lattice parameter up to 0.359 nm. At the same time, the XRD pattern (Fig. 10) still contains pronounced

diffraction peaks corresponding to molybdenum.

Fig. 9. Milling balls after mechanical alloying of the Ni–20 wt% Cr mixture in the Pulverisette 6 mill for 15 h

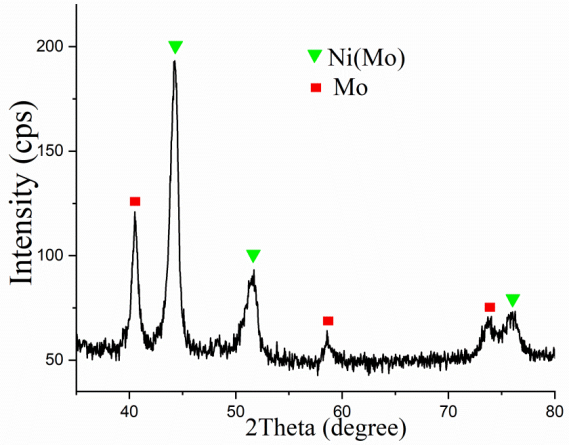

Fig. 10. XRD pattern of the Ni–20 wt% Mo powder obtained by mechanical alloying for 60 h in the Pulverisette 6 planetary mill

The SEM observations (Fig. 11) show that the agglomerates formed in the Ni–Mo system after 60 h of mechanical alloying possess a flake-like morphology and sizes ranging from 20 to 100 μm.

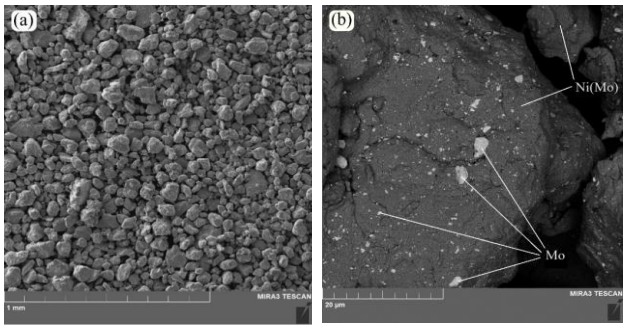

Fig. 11. SEM images of the Ni–20 wt% Mo powder obtained by mechanical alloying in the Pulverisette 6 planetary mill at a rotational speed of 400 rpm for 60 h

Thus, homogeneous Ni–Mo solid solutions were not obtained under the selected processing conditions. In addition to residual molybdenum, a significant amount of iron contamination was detected in the powders after 60 h of mechanical alloying.

During mechanical alloying in planetary mills, the initial stage of treatment is dominated by cold welding caused by intensive plastic deformation of powder particles under repeated impacts of the milling balls. This process is accompanied by particle flattening and rupture of surface oxide films. Accumulation of lattice defects and excess free energy during mechanical alloying promotes solid-state diffusion and accelerates phase formation. At later stages of treatment, local temperature increases inside the milling vial enhance diffusion processes at interphase boundaries and promote formation of substitutional solid solutions.

4. CONCLUSIONS

Comparative investigation of phase formation in Ni–20 wt% Cr and Ni–20 wt% Mo powder mixtures during vacuum synthesis and mechanical alloying was performed.

Vacuum heat treatment at 1200°C for 2 h resulted in formation of homogeneous FCC solid solutions in both systems due to diffusion of Cr or Mo into the Ni lattice.

Mechanical alloying behavior strongly depended on the alloying element. Homogeneous FCC Ni–20 wt% Cr solid solution powder was synthesized in the low-energy mode after 15 h of treatment in the Pulverisette 6 mill at 400 rpm. In contrast, complete homogenization of the Ni–20 wt% Mo system was not achieved even after 60 h of milling.

The slower alloying kinetics in the Ni–Mo system are associated with the larger atomic radius mismatch of molybdenum, and lower diffusion activity compared with chromium.

The obtained results of comparative behavior of the Ni–Cr and Ni–Mo systems in mechanical alloying and vacuum synthesis processes demonstrate that mechanical alloying is more effective for Ni–Cr powders, whereas vacuum synthesis is more suitable for obtaining homogeneous Ni–Mo solid solutions.

The obtained results may be useful for optimization of powder metallurgy routes for nickel-based refractory powder alloys.

REFERENCES

1. Sims CT, Stoloff NS, Hagel WC. Superalloys II: High-Temperature Materials for Aerospace and Industrial Power. New York: Wiley-Interscience; 1987.
2. Cherepova T, Dmitrieva G, Tisov O, Dukhota O, Kindrachuk M. Research on the properties of Co–TiC and Ni–TiC hip-sintered alloys. Acta Mechanica et Automatica. 2019;13(1): 57–67. https://doi.org/10.2478/ama-2019-0009
3. Wenbo Ma, Yubo Zhao, Łępicka M, Tisov O. Enhanced microstructure, mechanical, and tribological properties of Al, Ti, and nano-hBN-modified CoCrFeMnNi high-entropy alloy composites at elevated temperatures. Wear. 2025;572-573: 206055. https://doi.org/10.1016/j.wear.2025.206055
4. Mouritz A. Introduction to Aerospace Materials. Oxford: Woodhead Publishing Limited; 2012.
5. Okazaki M. High-temperature strength of Ni-base superalloy coatings. Science and Technology of Advanced Materials. 2000;2(2): 357–366. https://doi.org/10.1016/S1468-6996(00)00022-X
6. Chen S, Liu Z, Shen Y, Liu S. High-temperature corrosion of Ni–Cr–Mo cladding layers with different Si contents in NaCl–KCl–Na2SO4–K2SO4 mixed salt medium. Materials. 2022;15(9): 3152. https://doi.org/10.3390/ma15093152
7. Mediukh R, Mediukh V, Labunets V, Nosko P, Bashta O, Kondratenko I. Investigation of structure formation and tribotechnical properties of steel plasma coatings after chemical-heat treatment and liquid-phase impregnation. Acta Mechanica et Automatica. 2022;16(4): 382–7. https://doi.org/10.2478/ama-2022-0045
8. Kabátová M, Medyukh R, Kostenko V, Mihalik J, Seveíkova J. Secondary and finishing operations: improvement of corrosion and wear resistance of sintered steels by coating. European Congress and Exhibition on Powder Metallurgy. European PM Conference

DOI: 10.65731/ama/2026-0043

Proceedings. In Vienna. 2004;2: 423–6.
9. Medukh R, Kabatova M, Parilak L, Kostenko V, Dzubinsky M, Dudrova E. Microstructure and Properties of Layers Produced on Sintered Steels by Electrolytic Coatings and Diffusion Chroming. Int. Conference "Protective Coating 2002". Slovak Republic; 2002.
10. El-Bagoury N. Ni based superalloy: casting technology, metallurgy, development, properties and applications. International Journal of Engineering Sciences & Research Technology. 2016;5(2): 108–51.
11. Moyer JM, Jackman LA, Adasczik CB, Davis RM, Forbes-Jones R. Advances in triple melting superalloys 718, 706, and 720. In: Superalloys 718, 625, 706 and Various Derivatives. Ed. Loria EA. Warrendale: The Minerals, Metals and Materials Society. 1994; 39–48.
12. Wangyao P, Zrnik J, Vrchovinsky V, Novy Z, Kasanicka B. The analysis of creep behavior in an annealed nickel based alloy. The Journal of Metals, Materials and Minerals. 2022;12(2): 67–73.
13. Vrchovinský V, Zrnik J, Kvackaj T, Wangyao P. Effect of final cold rolled microstructures on creep deformation behavior in nickel base alloy. The Journal of Metals, Materials and Minerals. 2022;15(2): 57–68.
14. Wangyao P, Kvackaj T, Zrnik J, Vrchovinsky V, Novy Z. Effect of forming parameters on hot working process in nickel base alloy. The Journal of Metals, Materials and Minerals. 2022;13(2): 1–10.
15. Sreenu B, Sarkar R, Kumar SSS, Chatterjee S, Rao GA. Microstructure and mechanical behaviour of an advanced powder metallurgy nickel base superalloy processed through hot isostatic pressing route for aerospace applications. Materials Science and Engineering: A. 2020;797: 140254. https://doi.org/10.1016/j.msea.2020.140254
16. Suryanarayana C. Mechanical alloying and milling. Progress in Materials Science. 2001;46(1-2): 1–184. https://doi.org/10.1016/S0079-6425(99)00010-9
17. Bai Q, Lin J, Jiang J, Dean TA, Zou J, Tian G. A study of direct forging process for powder superalloys. Materials Science and Engineering: A. 2015;621: 68–75. https://doi.org/10.1016/j.msea.2014.10.039
18. López-Báez I, Martínez-Franko E, Zoz H, Trápaga-Martínez LG. Structural evolution of Ni–20Cr alloy during ball milling on elemental powders. Revista Mexicana de Fisica. 2011;57(2): 176–183.
19. Dekhil L, Hanneche N, Fellah M, Bououdina M, Mercier AM. Structural analysis and densification study of the mechanically alloyed Cr50Ni50 powders. The International Journal of Advanced Manufacturing Technology. 2020;108: 2515–24. https://doi.org/10.1007/s00170-020-05504-6
20. Oleszak D, Portnoy VK, Matyja H. Phase transformations in nanocrystalline mechanically alloyed Ni–Mo powders. Nanostructured Materials. 1999;12: 621–624. https://doi.org/10.1016/S0965-9773(99)00201-9
21. Oleszak D, Portnoy VK, Matyja H. Structure of mechanically alloyed Ni–Mo powders. Materials Science Forum. 1999;312–314: 345–50. https://doi.org/10.4028/www.scientific.net/MSF.312-314.345
22. Kud I, Ieremenko L, Uvarova I, Zyatkevich D. Features of the solid solution (Mo0.9,Cr0.1)Si2 formation depending on the state of initial mixture. American Journal of Materials Science. 2013;2(6): 202–209. https://doi.org/10.5923/j.materials.20120206.06
23. Uvarova I, Kud I, Yeremenko L, Lykhodid L, Ziatkevich D, Yarmola T. Sintering of powders in the CrSi2–Ti(Ta)Si2 systems depending on the methods of synthesis. Journal of the European Ceramic Society. 2010;30(14): 2947–53. https://doi.org/10.1016/j.jeurceramsoc.2010.05.026
24. Astakhov EA, Kud IV, Likhoded LS, Zyatkevich DP, Yakovleva MS, Eryomenko LI. Production of powders of the Ni–Cr–Al–Y system alloy doped with silicon by the powder metallurgy method. The Paton Welding Journal. 2010;3(6): 29–32.
25. Nash P. The Cr–Ni (chromium–nickel) system. Bulletin of Alloy Phase Diagrams. 1986;7(5): 466–76.
26. Hansen M, Anderko K. Constitution of Binary Alloys. New York: McGraw Hill; 1958.
27. Samsonov GV. Handbook of the Physicochemical Properties of the Elements. New York: Springer; 1968.

The authors would like to sincerely thank M. Skoryk from NanoMedTech for his help with the SEM-EDS analysis.

Iryna Kud: https://orcid.org/0000-0001-9903-1752

Roman Mediukh: https://orcid.org/0000-0003-2176-9321

Oleksandr Myslyvchenko: http://orcid.org/0000-0003-4903-6488

Roman Lytvyn: https://orcid.org/0000-0003-2087-8526

Larysa Krushynska: https://orcid.org/0000-0002-4110-8830

Vira Mediukh: https://orcid.org/0000-0003-1592-193X

Oleksandr Bashta: https://orcid.org/0000-0001-7914-897X

Pavlo Nosko: https://orcid.org/0000-0003-4792-6460

Ostap Zgalat-Lozynskyy: https://orcid.org/0000-0002-7013-5010